

FeNb magnetic properties correlated to microstructure features

M. Cherigui, S. Guessasma*, N. Fenineche, C. Coddet

Laboratoire d'Etudes et de Recherches sur les Matériaux, les Plasmas et les Surfaces (LERMPS), Université de Technologie de Belfort-Montbéliard (UTBM), Site de Sévenans, 90 010 Belfort Cedex, France

Received 2 February 2004; received in revised form 24 August 2004; accepted 13 September 2004

Abstract

We studied the effect of high-velocity oxy-fuel (HVOF) coating process parameters on magnetic properties of FeNb considering the role of coating microstructure. The present study was conducted using artificial neural network methodology. A first artificial neural network was optimized to relate process parameters to coating microstructure features. The effect of process parameters on magnetic properties was quantified by a second network. Predicted magnetic properties correlated to microstructure features were obtained using these optimized network structures. It was then possible to point out the role of microstructure for improvement coercivity, saturation magnetization and remanent magnetization.

© 2004 Elsevier B.V. All rights reserved.

Keywords: Magnetic measurement; Computer simulation; Artificial neural networks; FeNb; Thermal spray; High-velocity oxy-fuel thermal spray technique

1. Introduction

Magnetic materials underwent a great development in the 20th century [1]. Practical progress of magnetism largely depends on relevant advancement in coercivity control resulting from combined control of magnetocrystalline anisotropy and microstructure [1].

Amorphous materials can be used as alternative materials for magnetic material applications. These are obtained by a rapid quenching of metal from liquid to solid state with a cooling speed of about 10^6 K s^{-1} . They are characterized by long distance order absence of atomic arrangement and consequently they exhibit interesting mechanical, chemical and magnetic properties [2].

However, industrial applications related to these amorphous alloys have been restricted because of difficulties related to bulk material production.

Thermal spray can resolve this problem by considering rapid solidification of powder particles under high feed rates. In this study, we have used high-velocity oxy-fuel (HVOF) thermal spray technique. This process is adequate for spray-

ing low and intermediate melting temperature materials (e.g., polymers and metals). It permits to obtain high particle velocities needed for amorphization compared to other spray techniques.

In this study, FeNb alloy was chosen as feedstock material for its good aptitude to amorphization [3–5]. Literature is very poor on the use of such material as a feedstock for thermal spraying.

It is well known that microstructure, especially grain size, determine the hysteresis loop of a ferromagnetic material. Accordingly, magnetic softening should occur when structural correlation length or grain size becomes smaller than the ferromagnetic exchange length [6,7]. However, other factors can be associated to the magnetic softening when using thermal spray technology. These are mainly related to anisotropy of the layered structure, porosity level and phase content modification by evaporation.

In order to quantify the role of microstructure on FeNb magnetic properties, a model of data processing was considered based on artificial neural network methodology. Such methodology is an adequate tool for the study of complex processes with parameter interdependencies [8]. In addition, this technique proved to be applicable in the domain of mate-

* Corresponding author. Tel.: +33 3 84 58 31 29; fax: +33 3 84 58 32 86.
E-mail address: sofiane.guessasma@utbm.fr (S. Guessasma).

rials science [9] and especially in the case of thermal spraying [10].

In this study, two artificial neural networks (ANNs) were implemented as a tool of data analysis and prediction. A first ANN was built to correlate HVOF process parameters to phase contents and porosity level of FeNb coatings. A second ANN was considered to relate the same process parameters to coercivity, saturation magnetization and remanent magnetization.

2. Experimental procedure

2.1. Coating manufacturing

Thermal spraying of Fe₅₀Nb₅₀ (+0–44) powders was carried out using a commercial Sulzer Metco CDS HVOF spray system on copper substrates. Two substrate shapes were used: tubes (\varnothing 22 mm \times 1 mm) and sheets (70 mm \times 25 mm \times 1 mm). A gas mixture of oxygen and methane was used to produce the flame. The subsequent combustion of oxygen and methane produced a nominal flame temperature of 2500 K with a hypersonic velocity of about 2000 m s⁻¹. Experiments were carried out by varying two process parameters, namely methane fuel flow rate, V and spray distance, Z (distance separating the gun tip from the substrate plan). In addition, the cooling system was selected from either water or air system and thus represented the third variable, C . The other parameters were kept to a reference condition as shown in Table 1. After spraying, annealing treat-

Table 1
HVOF spray parameters

Parameter	Value
Spray gun	CDS 89443 psi
Oxygen gas flow rate (SLPM)	420
Methane fuel flow rate, V (SLPM)	145 , 200
Nitrogen carrier gas flow rate (SLPM)	20
Powder feed rate (g min ⁻¹)	35
Spray distance, Z (mm)	200 , 300
Substrate type	Cu sheet used with air cooling system, Cu tube used with water cooling system
Coating thickness (μ m)	200
Cooling system, C	water, air

Reference conditions are labelled with bold characters.

ment at 800 °C was carried out on samples in order to improve their magnetic properties.

2.2. Coating characterization

After metallographic preparation, cross-sections of FeNb coatings were analyzed using an optical microscope. The microstructure revealed tree features: porosity, dark grey and clear grey phases (Fig. 1). The dark phase ϕ_1 was rich on Nb element and the clear phase ϕ_2 on Fe element, as obtained by EDS analysis (Fig. 1b and c).

The percentage of each feature in the microstructure was calculated by image analysis using NIH image free software. These were porosity level, dark gray ϕ_1 and clear gray ϕ_2 zone percentages. Six images were used to assess mean and standard deviation associated to each feature. Magnetic mea-

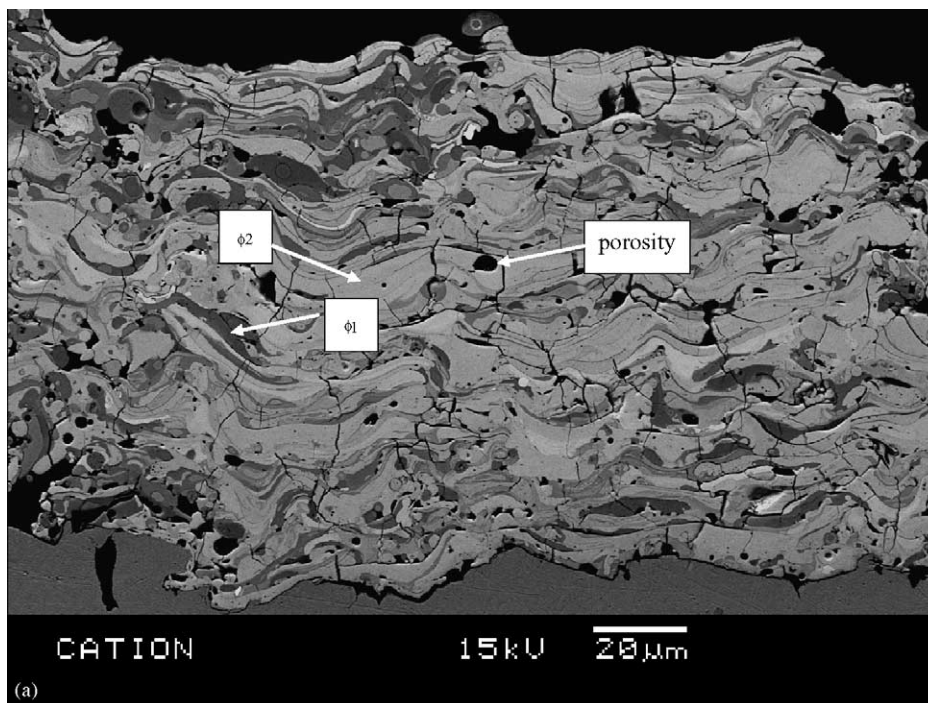


Fig. 1. Morphology and structure of FeNb coatings: (a) SEM image and EDS analysis of (b) dark grey zone ϕ_1 and (c) clear grey zone ϕ_2 .

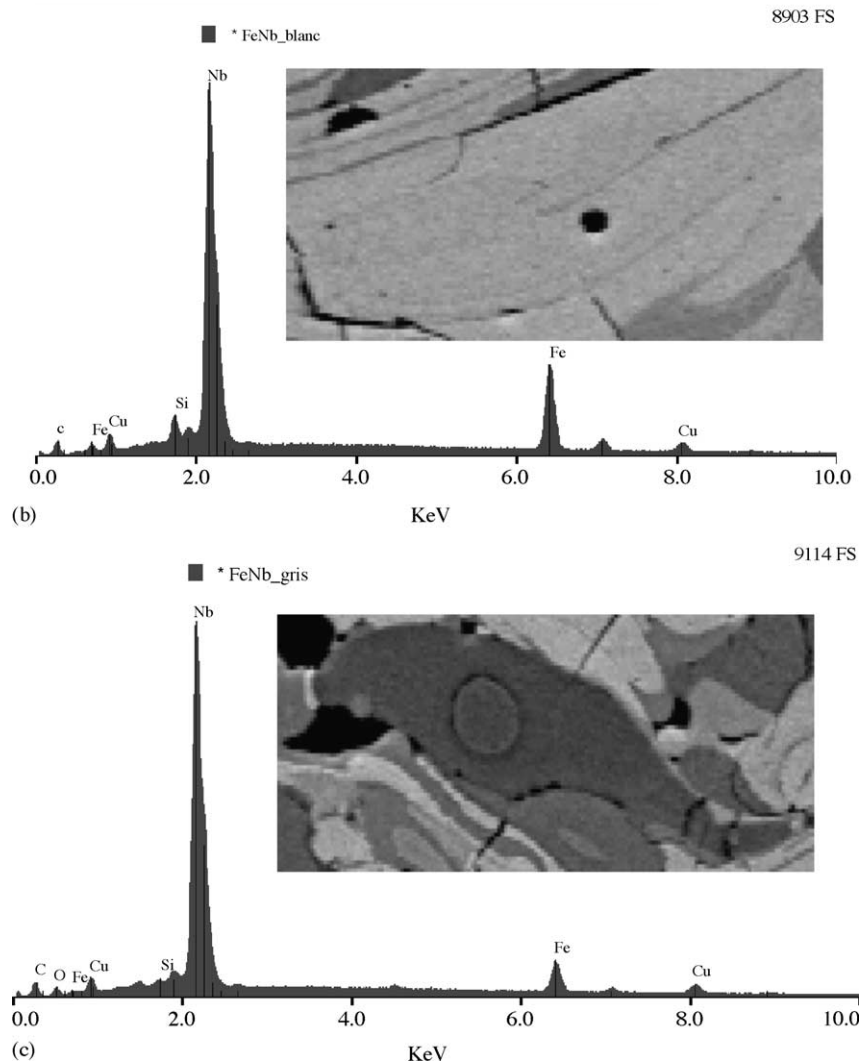


Fig. 1. (Continued).

measurements were realized using a hysteresis meter Bull M2000 SIIS, which enabled to draw the hysteresis loop of the considered samples. It permitted also to calculate magnetic properties, namely coercivity HC, saturation magnetization MS and remanent magnetization MR.

3. Simulation model

Artificial neural network (ANN) technique is a powerful statistical methodology used to recognize the correlations between the parameters of a given problem and its responses [8]. The correlations are recognized considering large but simple mathematical operations processed in/and between units called neurons, Fig. 3. For a detailed description of the use of this methodology, see for example [11].

In this study, two ANN structures were considered. The input pattern of these structures was the same and comprised three neurons. These were the spray distance, the fuel flow

rate and the cooling system. This last variable is considered as a classification category with state zero for air cooling system and one for water cooling system. The output pattern of the first structure comprised three neurons representing ϕ_1 , ϕ_2 and porosity content. The output pattern of the second structure is described also by three neurons, namely coercivity, saturation magnetization and remanent magnetization.

The input/output categories are related with a set of neurons organized in hidden layers (Fig. 2). Each neuron is connected with the other ones following well-established scheme. The strength of each connection is measured with a number called 'weight'. The neuron receives the weighted sum from the outputs of the other neurons and operates a non-linear transformation with the aid of a transfer function. It feeds the other neurons with the non-linear result until to reach the output pattern. In this study, a feedforward connection scheme between neurons was adopted for both structures [8]. In this scheme, each neuron of a given layer is connected to all neurons of the forward layer.

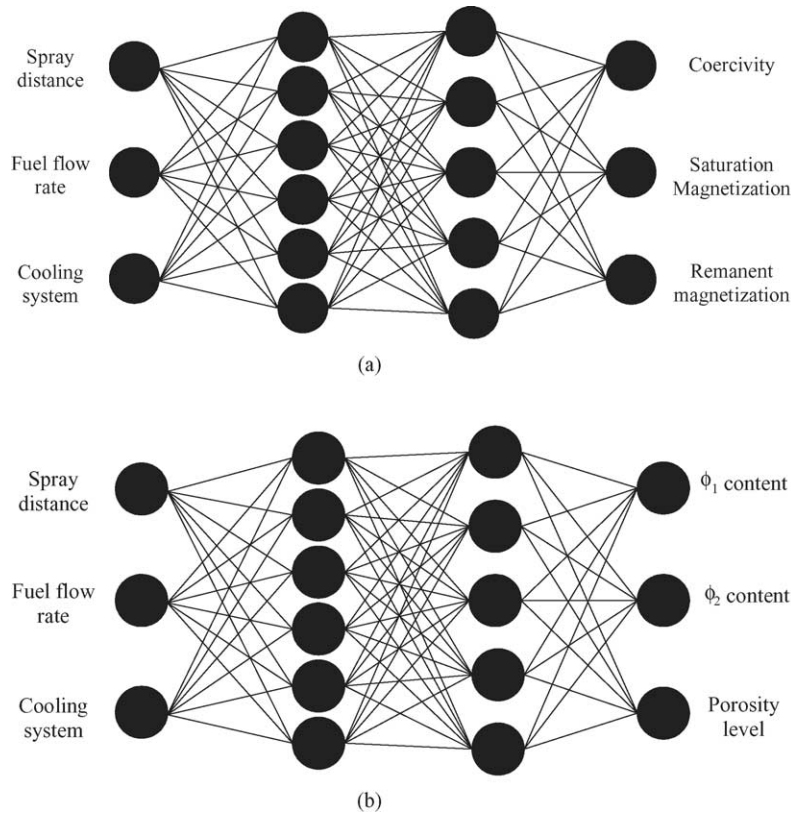


Fig. 2. Multilayer feedforward architectures considered in this study. (a) Optimized ANN structure relating process parameters to microstructure features, (b) optimized ANN structure relating process parameters to magnetic properties.

The optimization process consists in fixing the number of neurons and weight population in order to predict a response closer to experimental set result submitted to the ANN structure. Thus, the optimization requires a database and a training process to obtain generalization of ANN predicted results. The optimization steps are:

- Build the database considering mean variable values and associated standard deviation. Each variable is formatted between its admitted limits between 0 and 1. Each experimental set is enlarged 10 times considering its standard deviation [11].
- Divide the database into two categories: a training category required to tune weight population and a test category to test the validity of predicted results without modifying weight values.
- Start with an assumed weight population and a net structure.
- Submit to the structure a given number (i.e., batch size) of input/output examples from the database for training and testing.
- Correct weight values with the aid of a quick-propagation learning paradigm [12]. This paradigm backpropagates the error between the required and the predicted response in the net structure and modify the weight values to decrease this difference.
- Monitor training and test errors of the system output. Monitoring is associated to time limitation by considering a fixed cycle number of 2000.
- Add or remove neurons to decrease training and test errors.

4. Results and discussion

Optimization process revealed two ANN structures containing, for each one, two hidden layers as shown in Fig. 2. The overall error of training and test error was 0.005 and 0.05 for the first and second structures, respectively. The percentage of sample classification [13] was 100% for both structures, which means that all samples were learnt adequately by ANN structures. The overall error associated with the worst case was 0.0099 and 0.0868 for the first and second structures, respectively.

It was possible to obtain predicted evolution of each of the ANN responses as function of input categories. For example, when varying the spray distance in the first ANN structure, keeping the other parameters to a reference value, microstructure feature evolutions were obtained.

Fig. 3a shows an example of such evolutions in the case of porosity content. It is noticed that coating porosity decreases while spray distance increases from 150 to 270 mm. However, when the distance is larger than 270 mm, porosity level

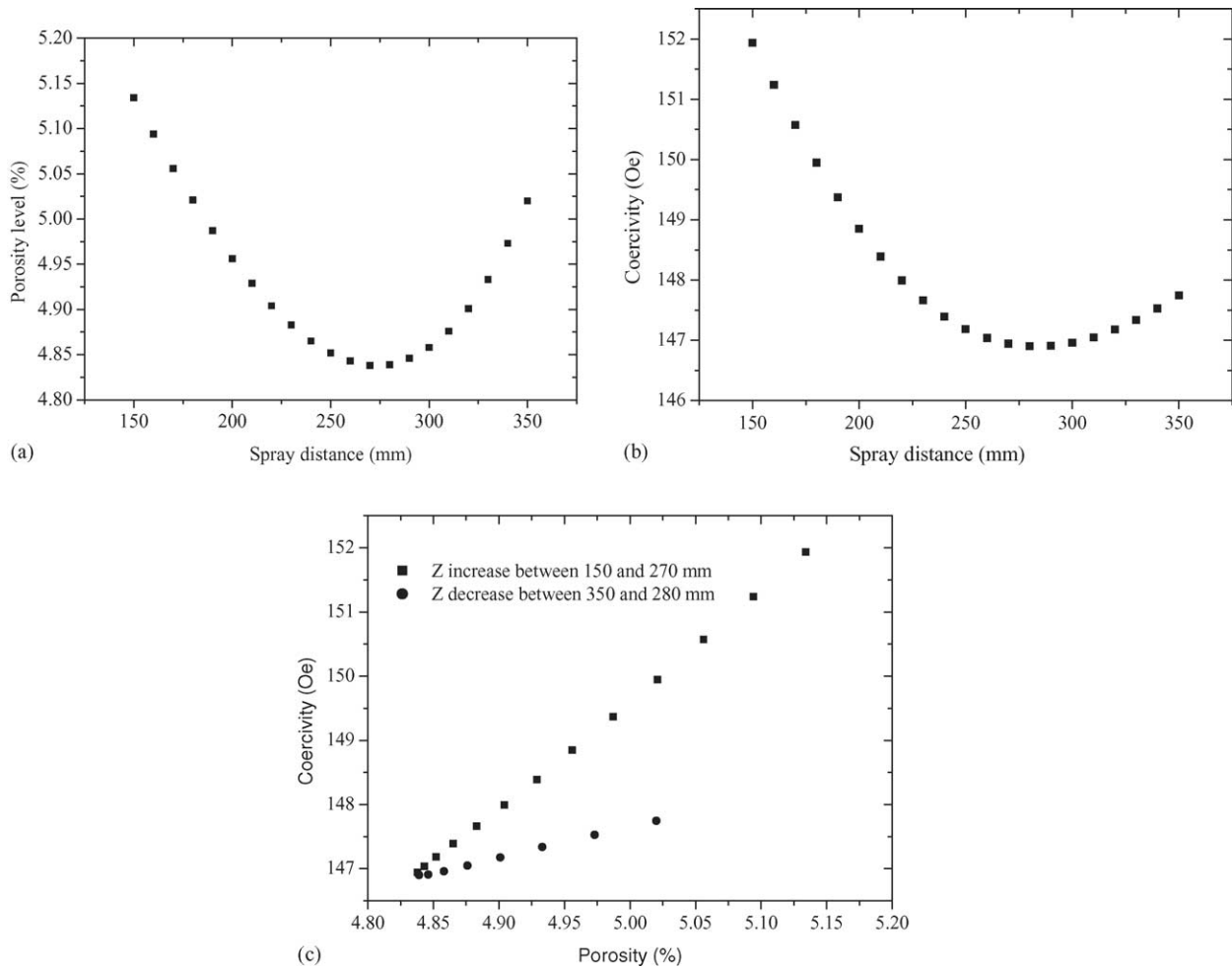


Fig. 3. (a) Porosity level predicted evolution vs. spray distance. (b) Predicted evolution of coercivity vs. spray distance. (c) Predicted evolution of coercivity vs. porosity level, considering spray distance effect. $V = 145$ SLPM, $C = 0$.

exhibits a rapid increase. This parabolic relationship can be explained considering particle temperature variation with respect to spray distance. Short spray distances are associated to short particle residence time in the flame. Consequently, they are less heated when they strike the substrate and thus cannot flatten adequately. This leads to a high porosity level in the coating [14,15]. For large spray distances, particles leave the flame and begin to solidify before they impinge the

substrate. Porosity level increases consequently for the same considerations.

As in the case of the first ANN structure, Fig. 3b illustrates an example of predicted curves when varying spray distance at the input pattern of the second ANN. This curve shows the variation of coating coercivity as function of spray distance. The same tendency as that of porosity level variation is noticed when spray distance increases. To explain such

Table 2

Measured microstructure features and magnetic properties associated to HVOF process parameters used in this study

Parameters			Microstructure features			Magnetic properties		
Z	V	C	P	ϕ_1	ϕ_2	HC	MS	MR
200	145	air	4.2 ± 1.54	19.6 ± 2.57	76.2 ± 1.52	137 ± 21.02	75.5 ± 7.54	16 ± 2.28
300	145	air	4 ± 1.36	19.5 ± 2.61	76.5 ± 1.76	136 ± 20.3	76 ± 7.81	16 ± 2.64
300	200	air	4.5 ± 1.07	19.1 ± 2.49	76.4 ± 1.58	136 ± 20.62	75.5 ± 7.45	16 ± 2.51
200	145	water	4 ± 1.30	19.2 ± 2.96	76.8 ± 1.08	137 ± 20.51	75.5 ± 7.44	15 ± 2.46
300	145	water	5 ± 1.50	19 ± 2.66	76 ± 1.58	138 ± 19.77	75 ± 7.6	15 ± 2.33
300	200	water	4.3 ± 1.25	19.3 ± 2.58	76.4 ± 1.09	138 ± 19.99	75.5 ± 7.53	15.5 ± 2.51

Z: spray distance; V: fuel flow rate; C: cooling system; P: porosity level; ϕ_1 : dark grey zone reach on Nb element; ϕ_2 : clear grey zone rich on Fe element. HC: coercivity; MS: saturation magnetization; MR: remanent magnetization.

Table 3
Predicted influence of microstructure features on magnetic properties associated to process parameter variations

Parameter	P			ϕ_2			ϕ_2		
	Z	V	C	Z	V	C	Z	V	C
HC	++ ↘ (17)	+↘ ↘ (10)	- ↘ (9)	+↘ ↘ (11)	- ↘ ↘ (9)	+↘ (7)	+↘ ↘ (13)	- ↘ ↘ (6)	+ ↘ (6)
MS	++ ↘ (15)	+↘ ↘ (2)	- ↘ (8)	+↘ (11)	- ↘ ↘ (2)	+↘ (6)	+↘ ↘ (12)	- ↘ ↘ (1)	+↘ (5)
MR	++ ↘ ↘ (1)	+↘ (2)	- ↘ (5)	+↘ (1)	- ↘ (3)	+↘ (5)	+↘ ↘ (1)	- ↘ (1)	+↘ (3)

Z: spray distance; V: fuel flow rate; C: cooling system; P: porosity level; ϕ_1 : dark grey zone reach on Nb element; ϕ_2 : clear grey zone rich on Fe element. HC: coercivity; MS: saturation magnetization; MR: remanent magnetization. ↘ or ↙ means increase or decrease of magnetic property when microstructure feature increases. + or - means increase or decrease of microstructure feature when process parameter increases. Number between brackets expresses relative variation of magnetic properties with respect to microstructure features.

correlation, one has to consider the effect of microstructure features as intermediate variables between process parameters and magnetic properties. Thus, for the same process parameter variation, responses are collected from the optimized ANN structures. In such a way, Fig. 3c shows coercivity response as a function of porosity level response. Linear increase of coercivity noticed is explained by the fact that porosity acts against the continuity of magnetic properties through the coating structure. These are considered as defects anchoring Bloch walls and involving consequently an increase of coercivity [16]. One can conclude that improvement of coercivity can be related to low porosity content and this is obtained when spray distance is around 275 mm. However, this improvement is not sufficiently significant to state that magnetic softening is important. This requires for example to take into account post-treatment conditions and especially the annealing time variation [17].

Fig. 4a shows the predicted variation of saturation magnetization as a function of porosity level. A low decrease of saturation magnetization is noticed. Generally, in magnetism studies, the decrease of this parameter is related to coercivity increase [18]. This is confirmed by our results as shown in Table 2. Fig. 4b shows the predicted evolution of remanent magnetization as function of porosity level. This last parameter exhibits weak variation compared to coercivity and saturation magnetization. In fact, this parameter is not well considered in studies dealing with magnetic applications because of its low sensitivity to process parameters.

Table 3 summarizes the effects of microstructure features on magnetic properties associated to process parameter variation.

Spray distance was the control factor of FeNb magnetic properties. It significantly modified coating microstructure features, which in turn controlled coercivity, saturation magnetisation and remanent magnetization.

Magnetic properties exhibited parabolic relationships with respect to fuel flow rate whatever was the process parameter type. This could be related to particle velocity and temperature variations. For low fuel flow rate, particle velocity and temperature could be associated to a low spray efficiency and consequently to degradation of magnetic properties. For high fuel flow rates, increase of particle velocity and evaporation could be related to the lowering of magnetic property values.

These effects are associated to a high porosity level and low phase contents.

However, porosity level controlled better magnetic properties compared to phase content parameters.

When changing cooling mode from air to water system, magnetic properties exhibited linear variations. Such evolutions are associated to the fact that this parameter was considered as a classification variable.

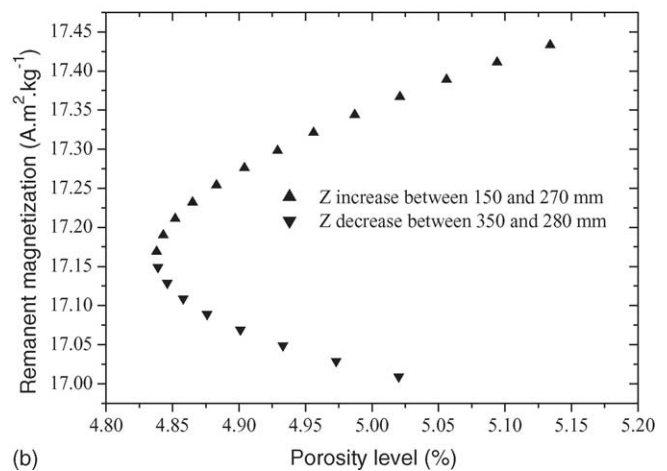
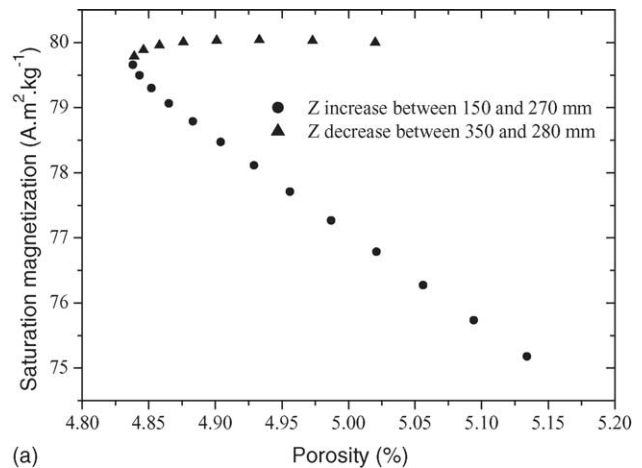


Fig. 4. Predicted evolutions of (a) saturation magnetization and (b) remanent magnetization vs. porosity level, considering spray distance effect. V = 145 SLPM, C = 0.

5. Summary and conclusions

Control of FeNb magnetic properties was investigated considering artificial neural networks. The role of microstructure was pointed out for explaining the effect of HVOF process parameters. Predicted results showed that spray distance was the most significant factor in modifying magnetic properties, especially coercivity and saturation magnetization. Variations larger than 10% on magnetic properties were predicted when varying spray distance between 150 and 350 mm. This parameter controlled also the microstructure including porosity level and phase content. Coercivity was the most influenced property compared to other magnetic properties when varying either fuel flow rate or cooling system.

Porosity level decrease was associated to improvement of coercivity, saturation magnetization and remanent magnetization.

References

- [1] J.M.D. Coey, *J. Alloys Compd.* 326 (2001) 2.
- [2] F.E. Luborsky, *Amorphous Metallic Alloys*, Butterworths, London, 1983.
- [3] N.E. Fenineche, M. Cherigui, A. Kellou, H. Aourag, C. Coddet, in: R. Marple, C. Moreau (Eds.), *Proceedings Advancing the Science and Applying the Technology*, ASM International, Materials Park, OH, USA, 2003, p. 1409.
- [4] N.E. Fenineche, M. Cherigui, H. Aourag, C. Coddet, *Mater. Lett.* 58 (2004) 1797.
- [5] M. Cherigui, H.I. Feraoun, N.E. Fenineche, H. Aourag, C. Coddet, *Mater. Chem. Phys.* 85 (2004) 113.
- [6] R. Alben, J.J. Becker, M.C. Chi, *J. Appl. Phys.* 49 (1978) 1653.
- [7] S.R. Kim, S.H. Lim, *J. Alloys Compd.* 258 (1997) 163.
- [8] M.M. Nelson, W.T. Illingworth, *A Practical Guide to Neural Nets*, third ed., Addison-Wesley Publishing, New York, USA, 1991.
- [9] H.K.D.H. Bhadeshia, *Neural Networks in Materials Science*, ISIJ International 39 (1999) 966.
- [10] S. Guessasma, G. Montavon, C. Coddet, in: E.F. Lugscheider (Ed.), *Proceedings of the International Thermal Spray Conference*, DVS-Verlag GmbH, Düsseldorf, Germany, 2002, p. 435.
- [11] S. Guessasma, G. Montavon, C. Coddet, *Comput. Mater. Sci.* 29 (2004) 315.
- [12] D. Patterson, *Artificial Neural Networks*, Prentice Hall, Singapore, 1996.
- [13] S. Guessasma, G. Montavon, P. Gougeon, C. Coddet, in: *Proceedings of the 3rd International Thermal Spray Conference*, DVS-Verlag GmbH, Düsseldorf, Germany, 2002, p. 453.
- [14] V.V. Sobolev, J.M. Guilemany, *Mater. Lett.* 18 (1994) 304.
- [15] L. Zhao, M. Parco, E. Lugscheider, *Surf. Coat. Technol.* 184 (2004) 298.
- [16] M. Nacken, W. Heller, *Arch. Eisenhuettenw.* 31 (1960) 153.
- [17] R. Houssa, V. Franco, A. Conde, *J. Magn. Magn. Mater.* 203 (1999) 199.
- [18] R.M. Bozorth, H.J. Williams, *Rev. Mod. Phys.* 17 (1945) 72.